49th AIAA Aerospace Sciences Meeting including the New Horizons Forum and Aerospace Exposition
4 - 7 January 2011, Orlando, Florida
AIAA 2011-487

Flow Separation Control over an Airfoil with Nanosecond Pulse Driven DBD Plasma Actuators

C. Rethmel[1]
The Ohio State University, Columbus, Ohio, 43235

J. Little[2]
University of Arizona, Tucson, Arizona, 85721

K. Takashima[3], A. Sinha[4], I. Adamovich[5] and M. Samimy[6]
The Ohio State University, Columbus, Ohio, 43235

This work continues an ongoing development and use of dielectric barrier discharge (DBD) plasma actuators driven by repetitive nanosecond pulses for high Reynolds number aerodynamic flow control. These actuators are believed to influence the flow via a thermal mechanism which is fundamentally different from the more commonly studied AC-DBD plasmas. Leading edge separation control on an 8-inch chord NACA 0015 airfoil is demonstrated at various post-stall angles of attack (α) for Reynolds numbers (Re) and Mach numbers (M) up to 1.15×10^6 and 0.26 respectively (free stream velocity, U_∞ = 93 m/s). The nanosecond pulse driven DBD can extend the stall angle at low Re by functioning as an active trip. At post-stall α, the device generates coherent spanwise vortices that transfer momentum from the freestream to the separated region, thus reattaching the flow. This is observed for all Re and M spanning the speed range of the subsonic tunnel used in this work. The actuator is also integrated into a feedback control system with a stagnation-line-sensing hot film on the airfoil pressure side. A simple on/off type controller that operates based on a threshold of the mean value of the power dissipated by the hot film is developed for this system. A preliminary extremum seeking controller is also investigated for dynamically varying Re. Several challenges typically associated with integration of DBD plasma actuators into a feedback control system have been overcome. The most important of these is the demonstration of control authority at realistic takeoff and landing Re and M.

Nomenclature

c = model chord, 20.32 cm
C_L = sectional lift coefficient

[1] Graduate student, Gas Dynamics and Turbulence Laboratory, Aeronautical and Astronautical Research Laboratories, Department of Mechanical and Aerospace Engineering, AIAA Student Member.
[2] Assistant Professor, Department of Aerospace and Mechanical Engineering, AIAA Member.
[3] Post-doctoral researcher, Nonequilibrium Thermodynamics Laboratory, Department of Mechanical and Aerospace Engineering, AIAA Member.
[4] PhD candidate, Gas Dynamics and Turbulence Laboratory, Aeronautical and Astronautical Research Laboratories, Department of Mechanical and Aerospace Engineering, AIAA Student Member.
[5] Professor, Nonequilibrium Thermodynamics Laboratory, Department of Mechanical and Aerospace Engineering, AIAA Associate Fellow.
[6] The Howard D. Winbigler Professor of Engineering, Gas Dynamics and Turbulence Laboratory, Aeronautical and Astronautical Research Laboratories, Department of Mechanical and Aerospace Engineering, AIAA Fellow.

Copyright © 2011 by M. Samimy. Published by the American Institute of Aeronautics and Astronautics, Inc., with permission.

C_P = pressure coefficient
f = frequency
F^+ = reduced frequency based on model chord, fc/U_∞
LE = airfoil leading edge
M = freestream Mach number, U_∞/(freestream speed of sound)
Re = Reynolds number based on cord length, $U_\infty c/v$
U_∞ = freestream velocity
x/c = normalized streamwise coordinate
α = angle of attack in degrees
v = kinematic viscosity

I. Introduction

Flow separation control with periodic excitation is widely established as a successful actuation technique in many flow systems.[1] This active flow control technology has the potential to substantially decrease the manufacturing cost, weight and parasitic drag associated with many passive control systems that rely purely on geometric modifications to the aerodynamic surface.[2] Active flow control is also well-suited for use with feedback controllers, and the successful integration of these technologies has been demonstrated in various aerodynamic systems.[3-9]

The periodic excitation used for active flow control is often generated using oscillatory momentum devices that produce zero-net mass flux.[10] Momentum can be introduced by a variety of techniques, but the most common ones are piezoelectric, electromagnetic and electrostatic. In all of these cases, an electromechanical driver creates the oscillatory flow used for excitation. These devices are controlled through electrical signals and, compared to passive control, offer a significant reduction in weight, mechanical complexity and parasitic drag. Unfortunately, they possess limited bandwidth and are subject to mechanical failure because the electromechanical driver is usually operated at resonance to produce the large amplitude perturbations necessary for realizing control authority at practical flight speeds. Even when operated in this fashion, amplitude requirements are often not met, especially for cruise conditions where actuator momentum requirements are high.

Flow control with plasma actuation is appealing because these devices are entirely surface mounted, lack mechanical parts, and possess high bandwidth while requiring relatively low power. Dielectric Barrier Discharge (DBD) plasma actuators driven by AC waveforms (AC-DBD) are the most commonly used of these devices.[11] They have been widely used for controlling flow separation, particularly on the leading edge of airfoils in relatively low Re conditions ($Re \sim 10^5$ and $U_\infty \sim 30$ m/s),[12] but few demonstrations of this technology exist at higher Re and M. The control mechanism for AC-DBD plasma actuators arises from an electrohydrodynamic (EHD) effect. Collisions between the charged species in the plasma and neutral particles near the surface generate a low speed ($U_{max} < 10$ m/s) near-wall jet in quiescent air.[13] The momentum production of these devices is fundamentally restricted by ion density in the space-charge region of electric discharge,[14] which has limited their use at higher speeds to date, although continuous improvements are being made.[15]

Early reports suggest DBD plasma actuators driven by a different type of waveform could be a superior alternative in some systems. The construction of the device is analogous to the AC-DBD, but the discharge is driven by repetitive nanosecond duration pulses (NS-DBD). DBD plasma created using these waveforms has shown control authority for leading edge airfoil separation control up to $M = 0.74$.[16] The NS-DBD produces very low velocity in the neutral species and the control mechanism is believed to stem from rapid localized heating of the near surface gas layer.[16,19] This scenario is well-established for localized arc filament plasma actuators (LAFPAs) that are effective for controlling high Reynolds number and high-speed (subsonic/supersonic, cold/hot) jets in both experiments[17] and computations.[18]

This work continues further exploration of the use of dielectric barrier discharge plasma actuators driven by repetitive nanosecond pulses for aerodynamic flow control. The efficacy of NS-DBD pulses has previously been demonstrated on an airfoil leading edge up to $Re = 1\text{x}10^6$ (62 m/sec).[19] The current work extends the investigation to higher M (0.26, 93 m/s) and Re ($1.15\text{x}10^6$) using an 8 inch chord NACA 0015

airfoil commonly studied with active flow control. It also incorporates an actuator recessed in the airfoil mold line which minimizes surface discontinuities near the leading edge. The NS-DBD actuator is integrated into a feedback control system with stagnation-line-sensing hot films near the leading edge. These sensors can be used to identify the various critical points in the shear stress field and have recently been implemented in AC-DBD plasma feedback control studies of lift enhancement.[7] Two types of control systems are investigated. The first is a very simple on/off type controller that operates based on a mean hot film signal value threshold for static *Re* conditions. The second is an extremum-seeking controller that is tested by dynamically varying *Re*. The practical utility of these feedback controllers is not fully realized, possibly due to the unfavorable location of the feedback sensor. However, several of the challenges typically associated with DBD plasma actuators have been overcome. The most important of these is the demonstration of control authority at $Re > 10^6$ and $M > 0.2$. Many remaining challenges are currently being addressed.

II. Experimental Facilities and Techniques

All the experiments are performed in a closed, recirculating wind tunnel at the Gas Dynamics and Turbulence Laboratory that produces velocities of 3-95 m/s with free stream turbulence levels on the order of 0.25%. The tunnel has a test section of 61 x 61 x 122 cm^3 (2 x 2 x 4 ft^3) and includes a heat exchanger to regulate the flow temperature. The operating conditions of the tunnel are measured using static pressure taps at the inlet and exit of the contraction section with two sets of differential static pressure transducers (Omega Engineering, Inc. PX655-25DI and PX655-5DI). The static pressure measurements are displayed and acquired by the data acquisition system using two process meters (Omega Engineering, Inc. DP-25-E-A).

The model used in these experiments is a NACA0015 airfoil with a chord length of 20.32 cm (8 in) and a span of 61 cm (2 ft). The fiberglass model consists of two separate pieces; a trailing edge section and an interchangeable leading edge section (**Figure 1**). The seams produced by mating the forward and aft pieces have been located at $x/c = 75\%$ on the suction side and $x/c = 30\%$ on the pressure side to avoid disturbing the developing boundary layer near the leading edge (LE). Each piece of the model has a hollow spar that serves as a support structure and also allows vinyl tubing used in C_P measurements to exit the model. One leading edge section (LE-1) provides baseline performance data, by being designed per the standard NACA profile. A second leading edge section is constructed with a 0.030 inch recess wrapping around the leading edge from 10% chord length on the pressure side to 35% chord length on the suction side (LE-2). This recess allows a DBD plasma actuator to be flush-mounted near the leading edge, while avoiding any significant discontinuities on the surface. The two LE pieces are necessary for characterization since placement of an actuator on the model does not permit C_P, and subsequent C_L, measurements due to obstruction of pressure taps near the LE. Experiments are performed at angles of attack up to 20°, which corresponds to approximately 12% blockage. No blockage or wall-corrections have been used.

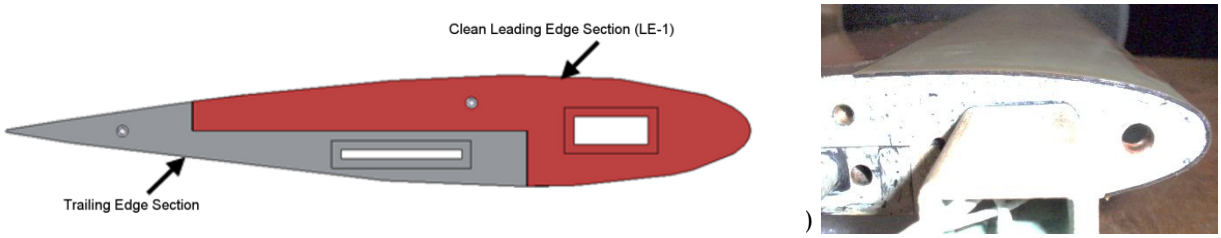

Figure 1: (a) Two-section airfoil, and (b) LE-2 with actuator installed in leading edge recess.

The airfoil is equipped with static pressure taps distributed around the chord near the center of the span. Static pressure measurements are acquired using Scanivalve digital pressure sensor arrays (DSA-3217). In post-processing, values of sectional C_P and C_L are averaged over 50 samples acquired at 1 Hz.

Six dynamic pressure transducers mounted flush with the surface of the suction side of the airfoil are capable of acquiring high-bandwidth pressure measurements. An array of Senflex® hot film sensors is adhered to the suction side of the airfoil from 37% to 63% chord length and on the pressure side from 11% to 17% chord length (**Figure 2** and **Figure 3**). A four-channel constant-voltage anemometer (Tao Systems, Inc.) provided the necessary excitation. The four-channel unit only permitted the use of four of the sensors, whose locations are shown in **Figure 2**. These devices respond to changes in the shear stress on the surface of the airfoil. The pressure side sensor at x/c = 11% is used to track movement of the stagnation line during closed-loop control. This is possible because shifts in the stagnation line are accompanied by corresponding shifts in the entire shear stress profile on the airfoil, which in turn results in a change in the power dissipated by the hot film sensor. This shift in the stagnation line can be correlated to changes in the static pressure distribution, and subsequently C_L.[7] The power dissipated (P_{HF}) by the hot film sensors is calculated using the resistance of the sensor and the applied constant voltage across the sensor. The resistance (R_{HF}) is calculated using the excitation voltage (V_w) and the measured sensor output voltage (V_s), which is low-pass filtered at 8 kHz, along with constants a and b which are specific to the data acquisition and signal conditioning hardware.

$$P_{HF} = \frac{V_w^2}{R_{HF}}, \qquad R_{HF} = \frac{1}{a\left(\frac{V_s}{V_w}\right) + b} \tag{1}$$

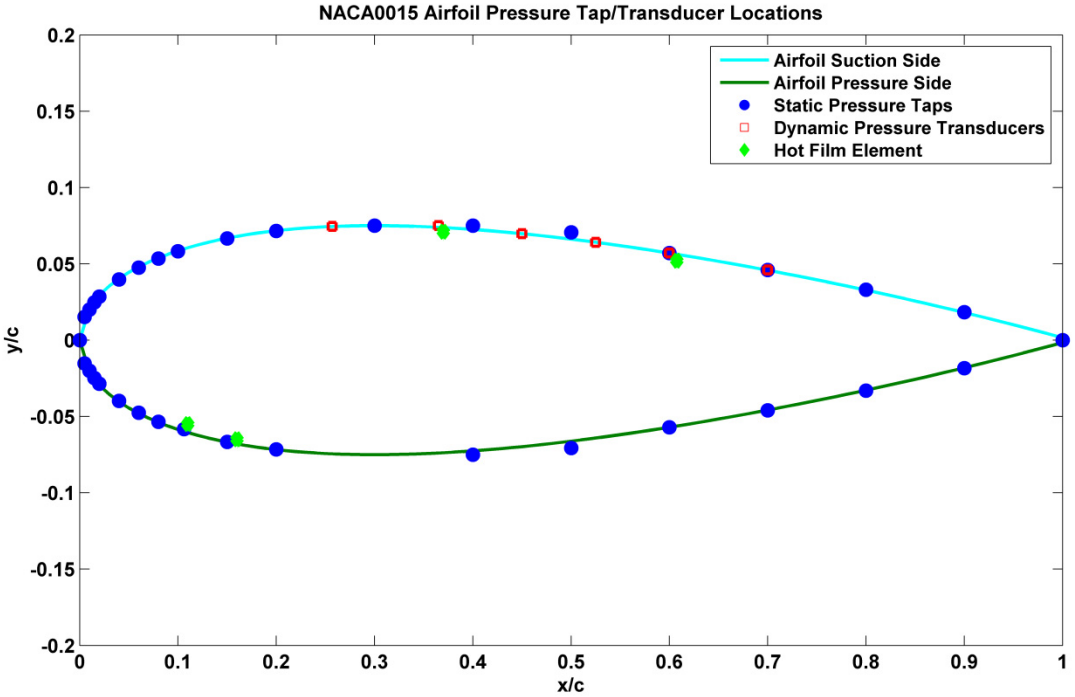

Figure 2: Instrumented airfoil schematic.

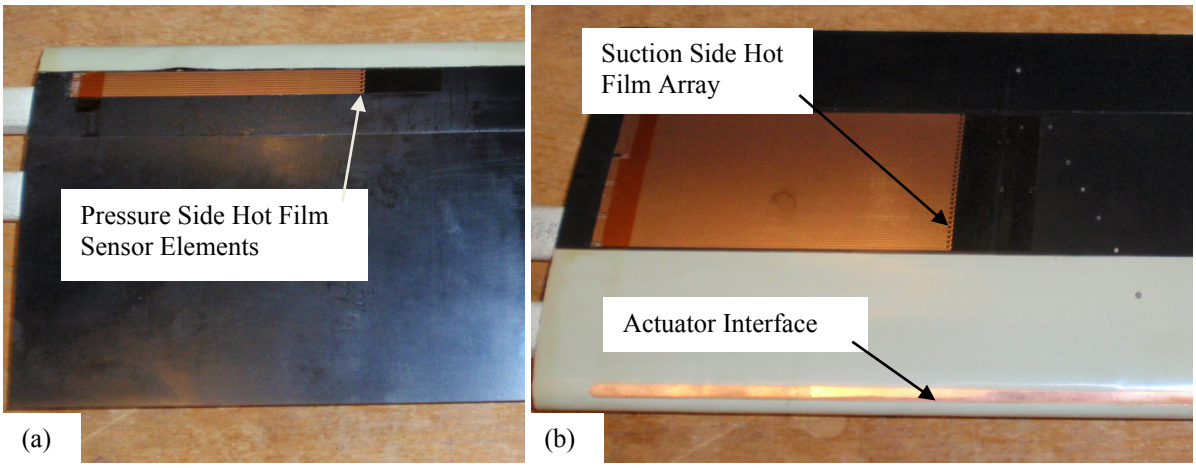

Figure 3: Leading edge recess airfoil with leading edge actuator installed (LE-2): view of (a) pressure side, and (b) suction side.

Two-component particle image velocimetry (PIV) is used to obtain quantitative measurements of the velocity field over the airfoil. Images are acquired and processed using a LaVision PIV system. Nominally submicron olive oil seed particles are introduced upstream of the test section contraction using a 6-jet atomizer. A dual-head Spectra Physics PIV-400 Nd:YAG laser is used in conjunction with spherical and cylindrical lenses to form a thin light sheet that allows PIV measurements. The time separation between laser pulses used for particle scattering is set according to the flow velocity, camera magnification and correlation window size. Two images corresponding to the pulses from each laser head are acquired by a LaVision 14 bit 2048 by 2048 pixel Imager Pro-X CCD camera equipped with a Nikon Nikkor 50 mm f/1.2 lens. For each image pair, subregions are cross-correlated using decreasing window size (64^2-32^2 pixels) multi-pass processing with 50% overlap. The resulting velocity fields are post-processed to remove spurious vectors using an allowable vector range and median filter. Removed vectors are replaced using an interpolation scheme based on the average of neighboring vectors. A 3x3 Gaussian smoothing filter is also applied to the calculated velocity fields. The PIV data are sampled at 10 Hz. Time-averaged statistics are calculated from 1000 instantaneous velocity fields.

Phase-locked PIV data are acquired using the programmable timing unit of the LaVision system. The acquisition is synced with the frequency of the actuation signal. Velocity fields at various phases of the actuator modulation frequency are investigated by stepping through the actuation period using time delays. The resulting phase-locked data sets are averaged over 100 images at each phase which is sufficient for resolving the primary features of the flow fields. Phase-locked PIV data is acquired at 5 Hz. The spatial resolution of PIV data for the airfoil is approximately 2.4 mm. The full-scale accuracy for all instantaneous velocity fields is found to be 0.9% assuming negligible laser timing errors and a correlation peak estimation error of 0.1 pixels.

The waveform used as the input for NS-DBD plasma is generated using an in-house constructed pulse generator. The pulser creates short duration pulses of approximately 100 ns FWHM. A sample of this waveform along with the respective power and dissipated energy is shown in **Figure 4**. The magnitude of the pulse varies with the input voltage to the pulser and DBD load. In this work, peak voltage is approximately 8.4 kV. **Figure 5** shows a phase-averaged schlieren image of a compression wave that is generated by the NS-DBD actuator. This compression wave is generated by the thermal effects of the plasma. The thermal effect is believed to be the main control mechanism in NS-DBD control, rather than the momentum addition in AC-DBD plasma actuation. The details of the plasma hardware and the physics of actuation have been discussed in our previous works.[19,20] Input signals for the NS-DBD plasma actuators are generated using a dSpace DSP 1103 board and corresponding software. Signals generated by dSpace are used as inputs to a Tektronix AF6310 function generator, which provides input signals to the pulse generator. The dSpace hardware and software are also used for closed-loop control.

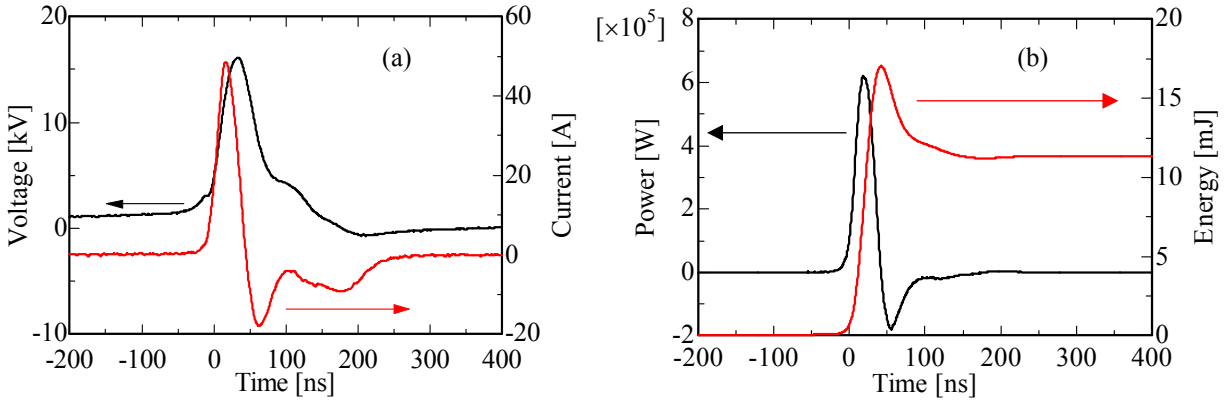

Figure 4: (a) Typical voltage and current, and (b) power and energy traces for an NS-DBD plasma actuator.

Figure 5: Schlieren image of a compression wave generated by NS-DBD plasma actuator viewed along the major axis of the actuator.

The DBD plasma actuators used in these experiments consist of asymmetric electrodes separated by a dielectric layer as shown in **Figure 6**. Two different types of actuators have been used. All open-loop control work presented here is performed using Kapton tape actuators. These actuators have electrodes made of copper tape with a dielectric layer of Kapton tape. The covered ground electrode is 12.7 mm (½ inch) wide and the exposed high voltage electrode is 6.35 mm (¼ in) wide. Both electrodes have thickness of 0.09 mm (3.5 mil). The dielectric barrier is composed of 3 layers of Kapton tape. Each layer has thickness of 0.09 mm (3.5 mil) and dielectric strength of 10 kV. Each layer of Kapton tape has a 0.04 mm (1.5 mil) layer of silicone adhesive such that the actual Kapton thickness for each tape layer is only 0.05 mm (2 mil). The total thicknesses of the dielectric and the device as a whole are 0.27 mm (10.5 mil) and 0.44 mm (17.5 mil), respectively. The dielectric is wrapped around the LE-2 recess to remove discontinuities (**Figure 3**). This actuator is also used for the extremum-seeking control work.

A printed circuit board (PCB) actuator is used with the on/off controller. Open-loop experiments have also been performed with this type of actuator, and results are qualitatively similar to those obtained with Kapton tape actuator. The PCB actuator is made of a polyimide dielectric clad in a copper laminate (Dupont Part FR8555R). This copper layer is etched away from the dielectric to produce the necessary electrode geometry. This leaves a single piece of 0.127 mm (5 mil) thick dielectric with a 0.025 mm (1 mil) copper electrode on each side arranged as seen in **Figure 6**. Going forward, the PCB actuators would be preferred for their improved repeatability of fabrication. For both types of actuators, the substrate consists of layers of Kapton tape necessary to fill the leading edge recess. These passive dielectric layers are necessary to make the top of the actuator flush with the airfoil mold line when installed. The recess is

intentionally designed in this fashion so thicker dielectrics could be employed in the future. The interface for both types of plasma actuators is set at x/c = 1% ± 0.49% with the plasma forming on the upstream side of the exposed electrode.

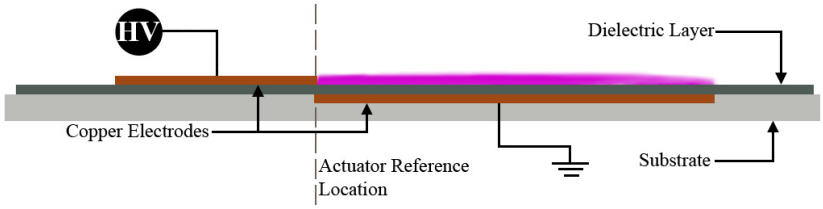

Figure 6: DBD plasma actuator schematic.

III. Results

A. Baseline Results

All the experiments are performed on the 8 inch chord NACA 0015 airfoil discussed above. Baseline characteristics are first determined using the leading edge with no recess (LE-1). C_P is integrated to calculate C_L as a function of α. $C_{L,max}$ is found around 12° for all Re, although the value of $C_{L,max}$ is dependent on Re as expected (**Figure 7**). This is most apparent by considering the change in performance between Re = 0.25x10^6 and 1.15x10^6 at α = 12-13°, where the low-Re behavior is most certainly caused by laminar boundary layer separation. The range of $C_{L,max}$ between all Re considered is 1.0-1.1. The post-stall form of the lift curve is strongly dependent on Re due to boundary layer transition at the LE. The different behaviors shown in **Figure 7** necessitate different control strategies depending on Re and α.

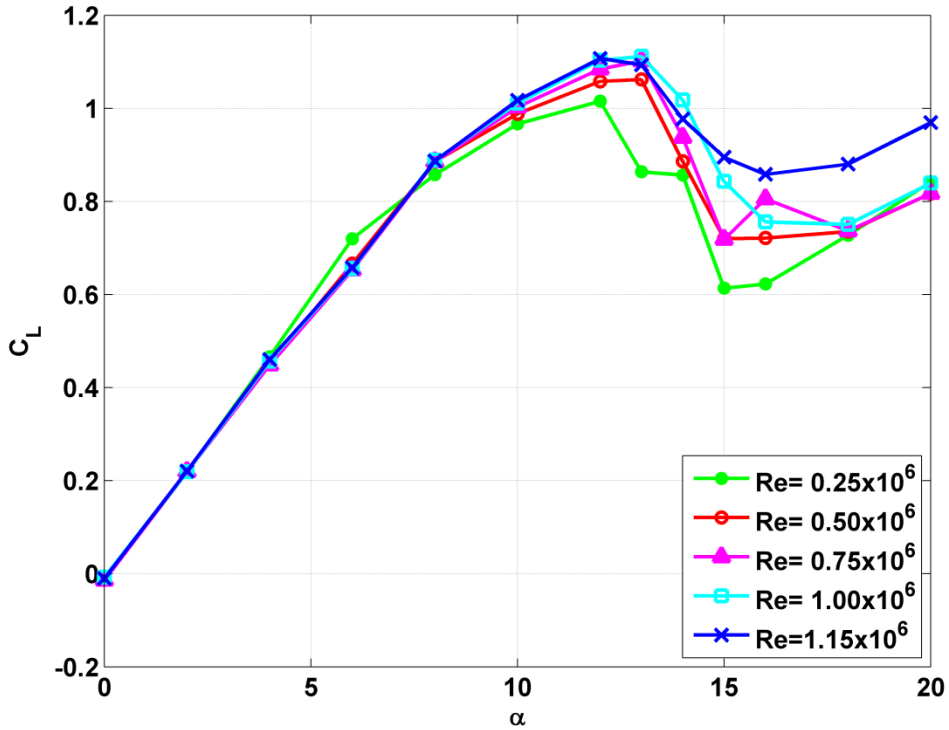

Figure 7: Lift coefficient vs. angle of attack for various Reynolds numbers for the baseline case.

A comparison between LE-1 and LE-2 without control is shown in **Figure 8**. This is done by installing an actuator on LE-2 with no plasma formation. This represents the passive effect of the DBD actuator on the airfoil C_P distribution. Four angles of attack and two actuators types are shown in **Figure 8**. No data is acquired at the LE in close proximity to the electrodes, but further downstream starting at x/c = 6%, holes are made in the dielectric to allow measurements. The change in LE surface condition has some effect on the baseline pressure distribution, but the overall differences are relatively minor. This comparison is also influenced by manual settings of angle of attack which have uncertainty of approximately ±1/4°. The data shown in **Figure 8** indicates that the actuator is not functioning as a passive control device and any control authority obtained is due to plasma formation.

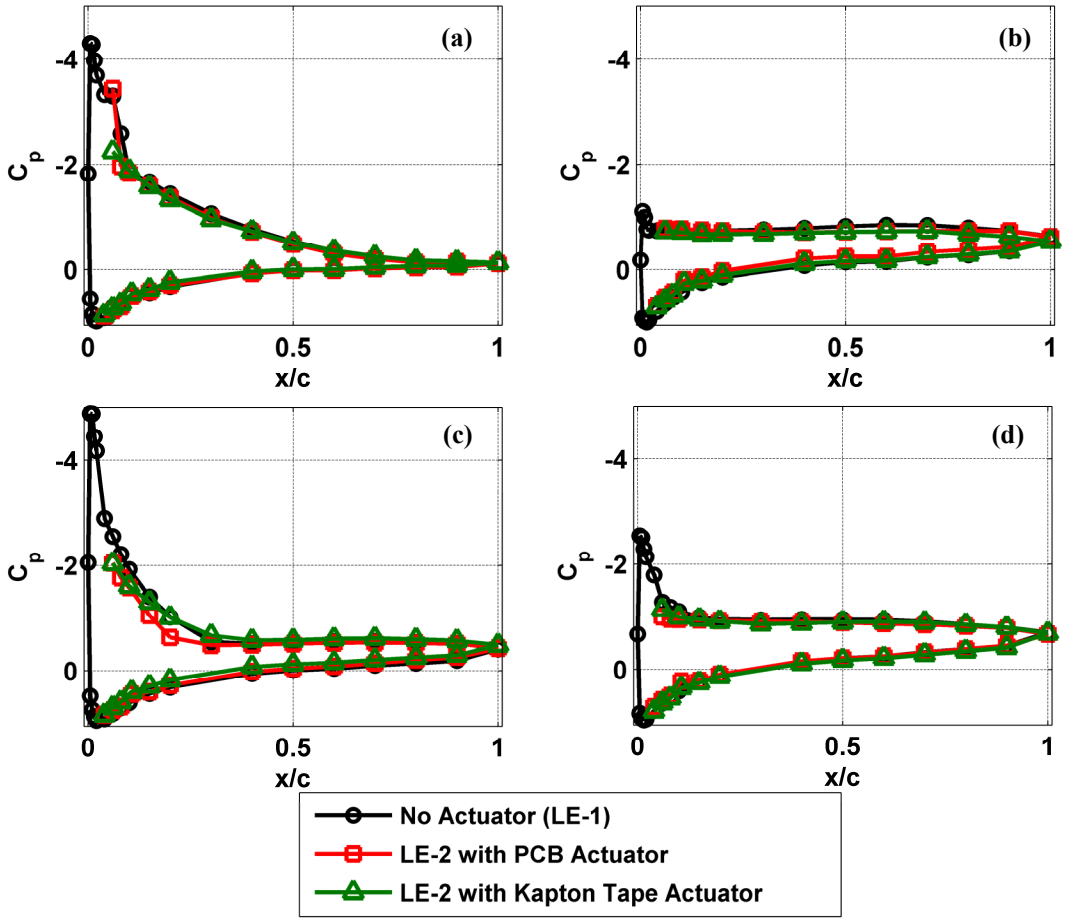

Figure 8: Baseline C_P comparison for clean airfoil (LE-1) and airfoil with recess and actuator (LE-2) (a) Re = 0.25x10^6, α = 12°, (b) Re = 0.25x10^6, α = 14°, (c) Re = 1.15x10^6, α = 14°, and (d) Re = 1.15x10^6, α = 16°.

B. Open-Loop Control

Open-loop characterization of both the actuator and the response of the hot film sensors is performed at various post stall α's. In all cases, the complete C_P distribution cannot be obtained due to installation of the actuator at the LE. Note that downstream of the electrodes, it is possible to create holes in the dielectric layer to allow measurements. Consequently, accurate C_L measurements are not possible because the largest changes in the lift are due to static pressure changes on the leading edge caused by the control. Therefore, the C_P value measured closest to the leading edge on the suction side will be used as an indicator of the change in C_L. A more negative value of C_P close to the leading edge should generally correspond to a higher lift.

A comparison between the effects of actuation with the PCB actuator and the Kapton tape actuator is shown in **Figure 9**. This is performed in order to assure that similar control authority is obtained for both types of actuators, and that the results of the two actuators can indeed be treated interchangeably. **Figure 9** shows that control authority, especially at high *Re* and α, is similar between the two types.

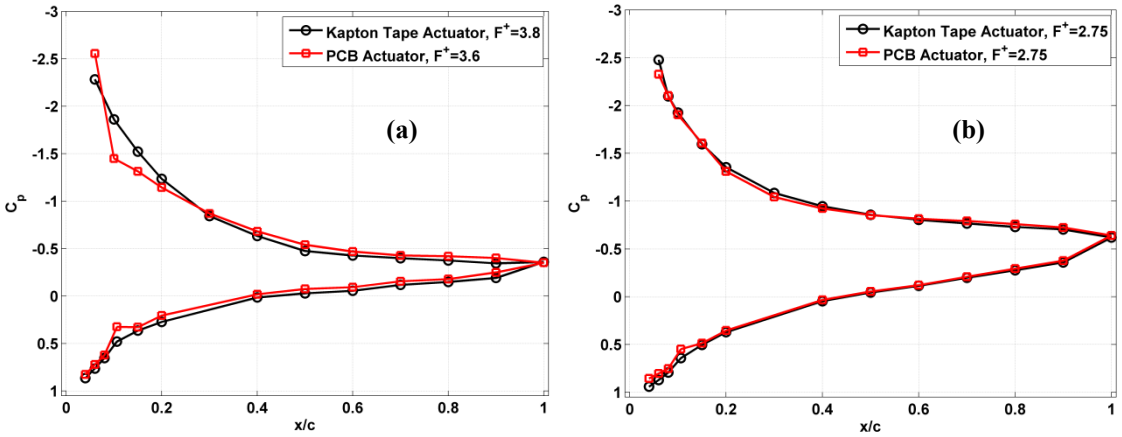

Figure 9: Controlled C_P comparison for airfoil with Kapton tape actuator and for airfoil with PCB actuator (a) $Re = 0.25\text{x}10^6$, $\alpha = 14°$, and (b) $Re = 1.15\text{x}10^6$, $\alpha = 20°$.

There are several different techniques for separation mitigation in airfoils. Examples include tripping the boundary layer in low Reynolds numbers, exciting the natural instabilities in the flow, and adding or removing momentum from the boundary layer via steady blowing/suction. Recent research has shown that NS-DBD actuators do not possess significant EHD effects.[16,19] Thus any effect due to a steady blowing can be ruled out. The remaining control mechanisms (boundary layer tripping and instability excitation) have been observed, depending on Reynolds number and angle of attack. Open-loop control results at two representative flow conditions for these mechanisms are shown in **Figure 10** and **Figure 11**. **Figure 10** presents a low *Re* ($0.25\text{x}10^6$) and a moderate α (14°) case. Sample C_P distributions as well as the response of both the static pressure near the LE on the suction side (x/c = 6%) and hot film at x/c = 11% on the pressure side are also provided. **Figure 10(a)** shows the baseline C_P distribution which is characterized by a near-zero pressure gradient on the suction side. Actuation at $F^+ = 2.5$ re-attaches the flow at the LE and moves the separation location to approximately x/c = 70%. In the present work, the hot film sensors are placed substantially aft of the stagnation line; yet a measureable correlation with suction side LE C_P can still be obtained (**Figure 10(b)**). The C_P data in **Figure 10(a)** shows that the stagnation line is at x/c < 5%; thus it is somewhat surprising that its motion is tracked at all so far downstream, especially with this low velocity flow. Examination of **Figure 10(b)** shows a negative correlation between suction side C_P and pressure side hot film near the LE. Note that baseline values are shown at $F^+ = 0$. This perceived negative correlation comes from the inverted C_P axis, and in actuality the correlation is positive. It is also important to recognize that the change in the hot film signal (~ 0.2 mW) is quite small compared to the nominal value (~ 85 mW). The response of C_P to forcing frequency is relatively constant from $F^+ = 2$ to $F^+ = 12$, and no preferred frequency can be distinguished. At higher frequency, the LE C_P value increases slightly indicating reduced control authority. These flow conditions (low-*Re*, moderate α) correspond to a case where a well-designed LE boundary layer trip can reattach the flow to the surface (see **Figure 7**). This, along with the lack of a preferred frequency in **Figure 10(b)**, suggests that the actuator functions as an active trip. This behavior has previously been observed for a different airfoil.[19]

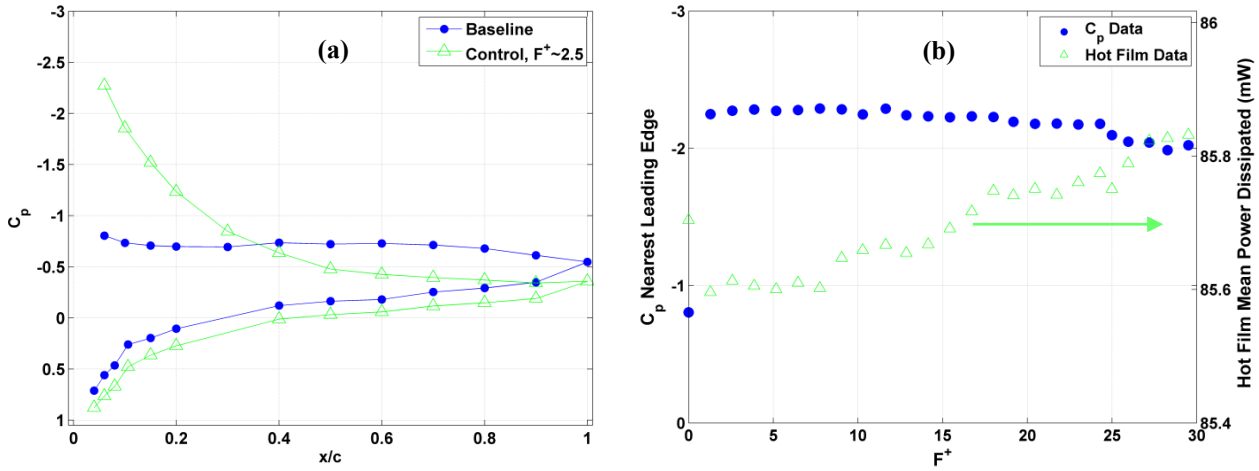

Figure 10: (a) C_P curves for baseline and with control at F^+ of 2.5, and (b) hot film mean dissipated power and C_P nearest leading edge for various forcing frequencies, for Re = 0.25x10^6, α = 14°.

Figure 11 considers the case of both high Re (1.15x10^6) and high α (18°). The baseline is characterized by deep stall. Actuation at F^+ = 1.9 reattaches flow to most of the suction surface (**Figure 11(a)**). The frequency sweep shown in **Figure 11(b)** is quite different from that previously examined for low Re (**Figure 10(b)**). A clear preference is seen for F^+ = 1.9, which is consistent with dimensionless frequencies observed in literature for most effective instability excitation ($F^+ \approx 1$).[21] This indicates a different physical mechanism. This is an important result which shows the efficacy of the NS-DBD plasma for controlling flow separation at Re = 1.15x10^6 and M = 0.26 (U_∞=93 m/s), associated with practical takeoff and landing conditions for transport aircraft, where the more common AC-DBD actuators are yet to show effectiveness. It is also in agreement with the results of Ref. 16, which used a shorter pulse width NS-DBD waveform with similar success. Correlation between suction side LE C_P and the hot film signal is substantially less apparent for these conditions. While the minimum for C_P occurs at F^+ = 1.9, the corresponding minimum for the hot film signal is near F^+ = 3-4, but there is substantial scatter in this hot film data. It is unclear if this is a result of the control mechanism or a characteristic of the hot film reaction to changes in the shear stress distribution.

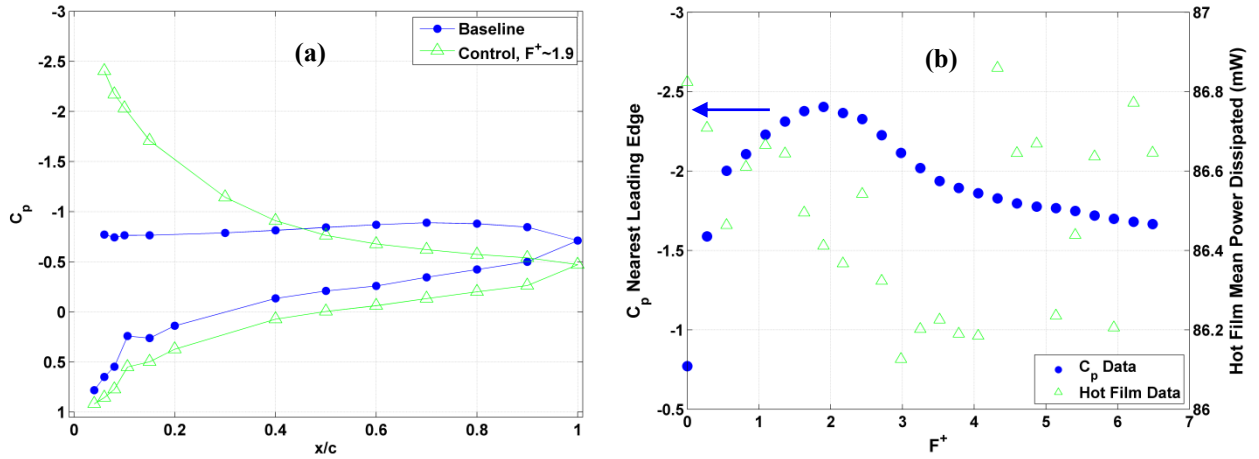

Figure 11: (a) C_P curves for baseline and with control at F^+ of 1.9, and (b) hot film mean dissipated power and C_P nearest leading edge for various forcing frequencies, for Re = 1.15x10^6, α = 18°.

The frequency sweeps of Figure 10 and 11 show two different control mechanisms are at play. In the low *Re* (0.25x10^6), low-α (14°) case, the frequency of actuation is not critical. This behavior indicates that no flow instabilities are being excited and the actuator is acting as an active boundary layer trip. The excitation of natural flow instabilities is largely dependent on the frequency of excitation. This is shown in **Figure 11** where a clear frequency preference of around $F^+ = 1.9$ is seen. This indicates that the primary method of control in these conditions could be the generation of large scale structures through the excitation of natural flow instabilities. The presence of structures in the flow is confirmed with PIV data. Coherent spanwise vortices can be identified using the phase-averaged fluctuating component of the vertical velocity together with the swirling strength, as discussed in our previous work.[19] **Figure 12(a)** shows the fluctuating *v*-velocity component, which indicates alternating areas of positive and negative v-velocity. Swirling strength (**Figure 12(b)**) confirms that adjacent pairs of these alternating regions constitute distinct vortices in the flow (seen at approximately *x*/*c* = 20% and 50%). These vortices entrain high momentum fluid into the separated region near the airfoil. This mechanism is widely established in the literature for controlling separation in many flow systems.[1] However, this behavior has not been demonstrated at these *Re* and *M* for more common AC-DBD plasma actuators. It should also be noted that spanwise vortices have been visualized over a range of actuation frequencies, which suggests that this device has high bandwidth. It is believed that this mechanism stems from rapid localized heating of the near-surface flow by the plasma. This produces local compression waves similar to LAFPAs that have shown control authority for various high *Re* and high *M* jets.[17]

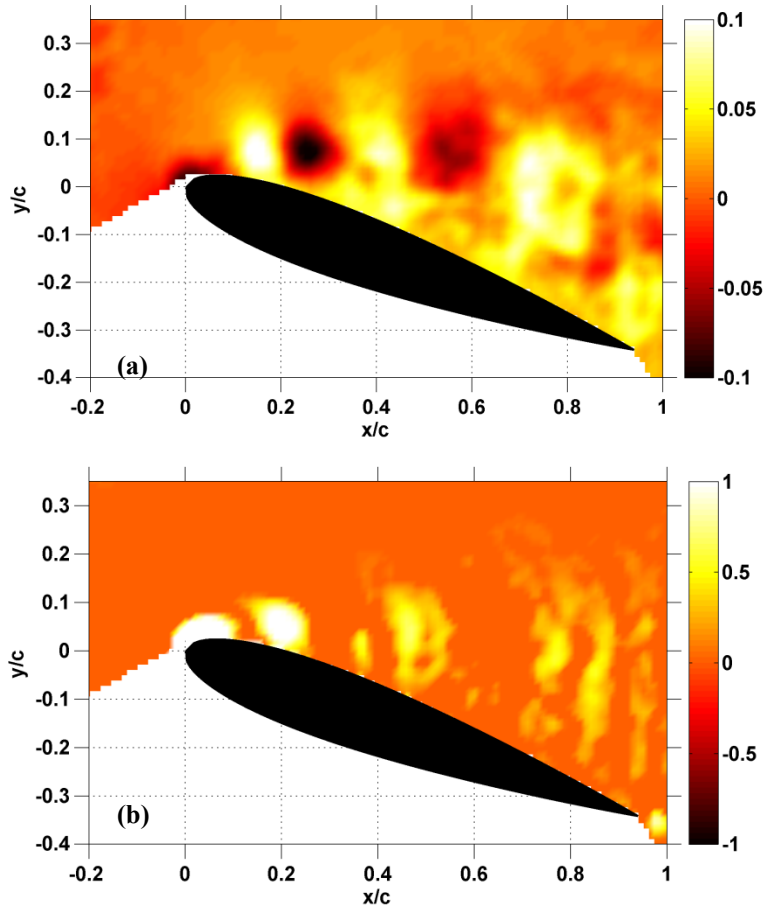

Figure 12: (a) Phase-averaged fluctuating *v*-velocity component (normalized by U_∞), and (b) normalized swirling strength, for *Re* = 1.15x10^6, α = 20°, F^+ = 1.9.

C. Closed-Loop Control

Closed-loop control is investigated over a range of *Re* and α. The signal from the hot film sensor nearest the LE is used as the input to the controller. This sensor is as close to the leading edge as one can possibly instrument for the given actuator geometry, and is the same sensor used to collect the data presented in **Figure 10(b)** and **Figure 11(b)**. It is used to obtain a relative estimate of the stagnation point location near the leading edge of the airfoil, which is approximately correlated to C_L, as discussed earlier. Since the performance of feedback control crucially depends on the quality of the measured signal employed as a surrogate for the performance objective, better results might be expected if sensors could be placed closer to the stagnation point. For example, in Ref. 7 a hot film sensor at $x/c = 0.17\%$ indicated increasing shear stress with increasing C_L. Both the strength and sign of this correlation are dependent on the sensor location, because very near the stagnation point the flow changes are severe, but become more gradual with increasing chordwise distance.[7]

Two types of controllers are explored using hot films. The first is an on/off controller based on the mean value of the power dissipated by the hot-film, which acts as the 'decision variable'. **Figure 13** depicts its schematic. In this case, a nominal threshold and a dead zone width are set based on experience gained in previous open-loop experiments. These settings are such that a reading of dissipated power above the dead zone indicates separated flow, whereas one below it indicates attached flow (**Figure 10(b)**). A dead zone is used rather than a single threshold value to avoid unsteadiness for measured values very near the nominal threshold. Note that the actuator, if it is indeed commanded to operate, runs at a preset frequency *f* that is deemed optimal from the open-loop control results. The responsiveness of the controller is determined by the length of time over which raw hot-film voltage measurements must be accumulated for the necessary statistics (average of dissipated power, in this case) to converge. This time interval is typically a function of the flow time step, but in all the experiments reported here, it was set to 0.1 s (10 to 45 flow time steps, depending on *Re*). The processed value is held over this interval, while the running sum is computed. At the end of each interval, the processed value is refreshed, and the running sum is reset to 0.

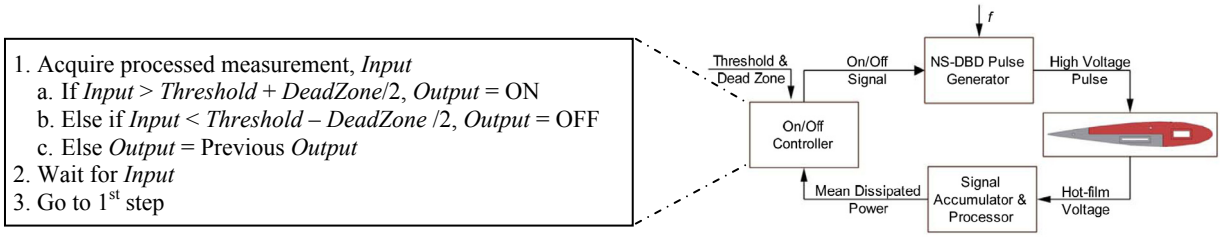

Figure 13: The on/off control scheme.

On/off control is demonstrated at $Re = 0.25 \times 10^6$ and $\alpha = 14°$. Hysteresis effects are significant in this flow regime, meaning that once flow is attached by actuation it can remain attached for some time even with the actuator switched off.[22] When this is the case, it is advantageous to temporarily turn the actuator off to conserve power and then reinitiate the plasma when the flow is once again beginning to separate. This behavior is demonstrated in **Figure 14**. The dSpace controller clock is running at 50 kHz, so that the raw sensor voltage is sampled at this rate and the decision step (Step 1 in **Figure 13**) is performed in 20 µs. The sensing and its online processing are initiated before time $t = 0$ on the graph. When the controller is activated at $t = 1.5$ s, this processed measurement is found to be above the dead zone, and the actuator is enabled within 20 µs. The flow gets attached within the next 0.2 s, and sensing the corresponding drop in the dissipated power, the controller switches off the actuator (indicated by the flat-lining pulser input signal). From $t = 1.5$ s to 2.75 s, the hysteresis effect causes the flow to remain attached, which is continuously verified by the controller. The flow starts to separate again at $t = 2.75$ s, at which time the controller turns the actuator on to keep the flow attached to the airfoil, and the cycle is repeated. This behavior is consistent with the control mechanism observed in **Figure 10** (i.e. transition).

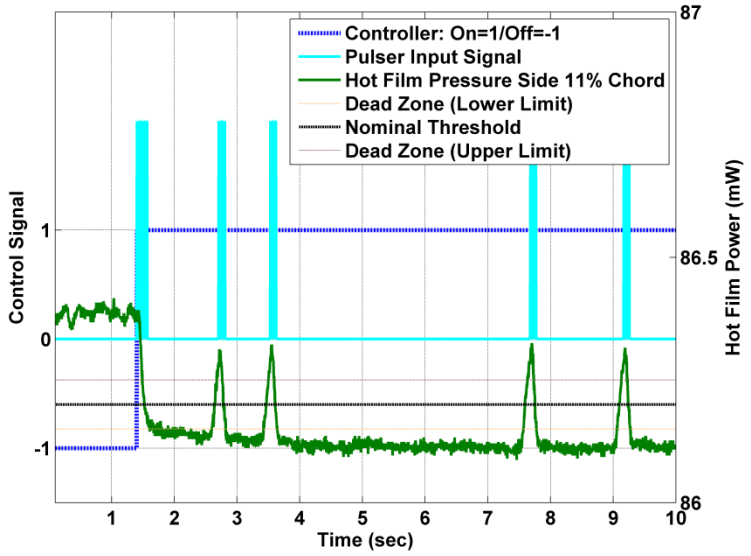

Figure 14: On/off controller at $Re = 0.25 \times 10^6$, $\alpha = 14°$.

When the on/off controller is operated outside of the range where hysteresis effects are present (high α), the plasma must continuously run at the preset frequency to keep the flow attached. If the actuator were to switch on and off repeatedly, then the resulting disruption to the large-scale vortex pattern (see **Figure 12**) would create large unsteady forces on the airfoil. Therefore, for these flow conditions, the threshold for the on/off controller is intentionally set low. Thus the controller deems the flow to be separated at all times, and the actuator remains enabled until the controller is manually disabled. For clarity the nanosecond pulser signal is not included in **Figure 15** because it is operating at the predetermined frequency of $F^+ = 2.75$ whenever the controller is enabled.

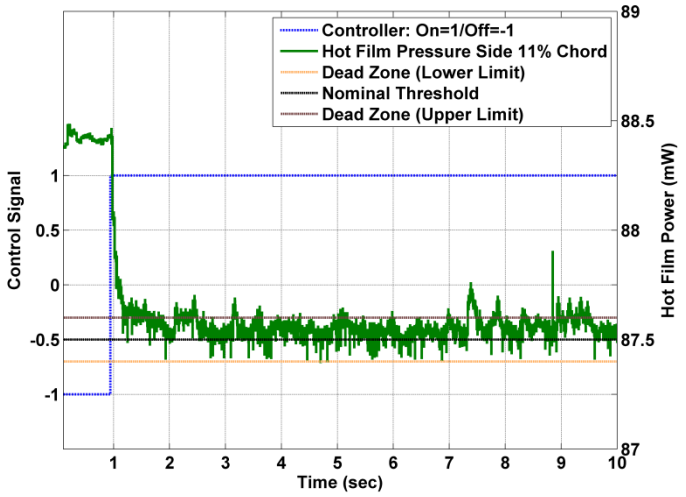

Figure 15: On/off controller at $Re = 1.15 \times 10^6$, $\alpha = 20°$.

Although closed-loop control using an on/off controller is successful, several issues have been encountered. The mean of the hot film data slowly drifts over extended periods of constant flow conditions resulting in controller inconsistency. The reason for this drift is unknown as it occurs regardless of whether the plasma is on or off and persists throughout the testing. This is especially problematic since the sensitivity of the hot film to C_L changes at $x/c = 11\%$ is quite small. Consequently,

the threshold had to be manually set for each control run, although the dead zone width could be retained constant.

It should be noted that the NS-DBD plasma creates substantial electro-magnetic interference (EMI). This is seen in **Figure 16** as impulse-like spikes in the time trace, which effectively represent the HV pulse (100 ns). These spikes cannot be removed by standard filtering in the frequency domain since they manifest as broadband signal noise. Instead, a 12-point median filter is employed in the time domain to minimize its effect on the processed signal; an example is shown in **Figure 16**. This is implemented within the signal processing block in **Figure 13.** It should be noted that all cabling and connections are carefully shielded and multiple ferrites are employed before using these signal processing techniques.

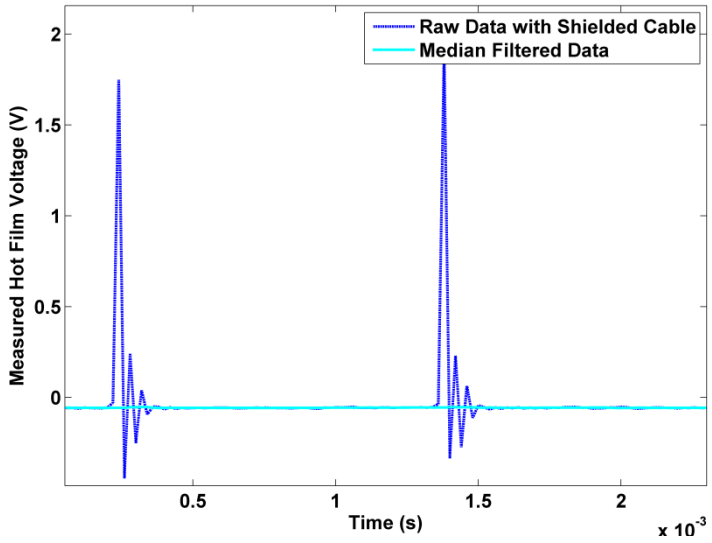

Figure 16: Hot film median filter signal processing example.

Some preliminary work using extremum-seeking control has also been attempted using the hot film sensors. This controller searches for an extremum (a maximum or a minimum) in the performance objective by continuously adjusting a chosen parameter of the actuation. The extremum-seeking controller is based on the Modified Nelder-Mead Algorithm implemented previously in a high Reynolds number high-speed jet forced with localized arc filament plasma actuators.[8] In brief, after each update of the actuation parameter of interest, the measured change in the performance objective is used to decide the sign and magnitude of the next update. In the present implementation, the objective is to keep C_L maximized by optimizing the forcing frequency of the NS-DBD plasma actuator, even when the flow speed is dynamically varied. Since C_L cannot be measured in real-time, one has to improvise with the surrogate objective of minimizing the power dissipated by the leading edge hot film sensor (see **Figure 10** and **Figure 11**). However, it is shown in **Figure 10** and **Figure 11** that the minimum of this quantity does not necessarily correspond directly to the minimum of the C_P value near the leading edge. This means that although using the extremum-seeking controller with the hot films may result in an increase in C_L compared to the baseline case, one cannot guarantee convergence to the optimal forcing frequency determined from the open-loop frequency sweep. The hot film data also shows that, in the range of control frequencies explored, there are several local minima and areas of relatively flat frequency response. This leads to inconsistency in the extremum-seeking controller because it is difficult for it to navigate through these frequency ranges.

The inconsistency of the extremum-seeking controller is shown in **Figure 17** and **Figure 18**. In these cases, the angle of attack is held at 18° and the Reynolds number is varied during the run from $Re = 0.25\text{x}10^6$ to $Re = 1.15\text{x}10^6$ and back. These changes occurred over a time period of 90 seconds, and this is determined by the responsiveness of the wind tunnel flow control system. It should be noted that

separation control via boundary layer transition has not been observed at this angle of attack and a preferred frequency does exist in the sweep data (see **Figure 11(b)**). These two figures correspond to two consecutive runs with the same controller parameters and flow conditions. The extremum-seeking controller is unable to produce repeatable results, presumably due to the limited sensitivity of the hot film at its present location. In both runs, at a time of approximately 350 seconds the controller loses control authority as a result of a spike in the actuation frequency. In **Figure 18**, the controller is able to navigate through this spike and ultimately settle upon the optimal forcing frequency, but in **Figure 17** the controller continues forcing at a frequency which is too high. We postulate that if the hot film sensor used for closed-loop control could be placed closer to the stagnation line, the consistency of the controllers could be improved. This has been previously shown for simple on/off controllers with sensors located at $x/c = 0.17\%$.[7] In our experiments, this is not possible due to the location of the actuator recess, which is designed to provide adequate spacing between the hot films and electrodes to prevent equipment damage. If these fragile sensors were mounted on the dielectric even away from the electrodes they would be irrevocably damaged by physically changing the actuator. Despite the implementation issues with extremum-seeking control, it is encouraging to see control authority at the *Re* and *M* conditions considered here, which represent the maximum capabilities of the employed wind tunnel.

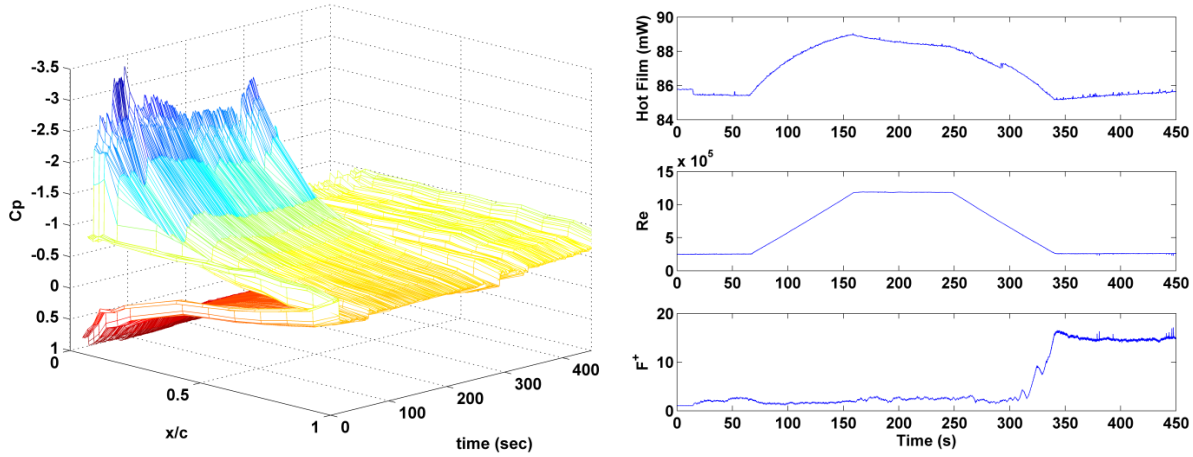

Figure 17: Extremum-seeking control: *Re* varied from 0.25x10^6 to 1.15x10^6 to 0.25x10^6, α = 18°.

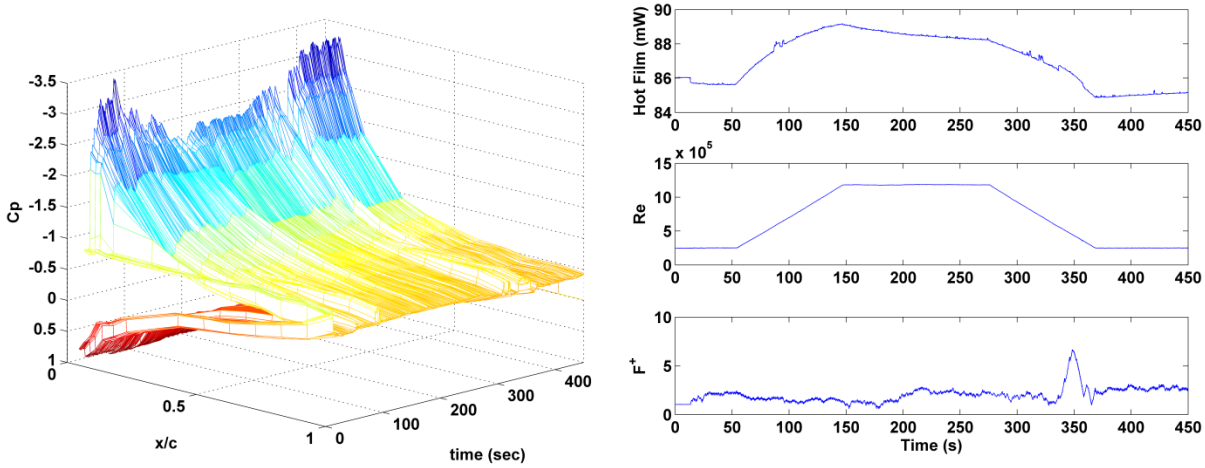

Figure 18: Performance of extremum-seeking control during a different run using the same parameters as in Figure 17.

IV. Conclusions

This work presents our continued development and use of dielectric barrier discharge (DBD) plasma actuators driven by repetitive nanosecond pulses in high Reynolds number aerodynamic flow control. Leading edge separation control on an 8-inch chord NACA 0015 airfoil is demonstrated at various post-stall angles of attack (α) for Reynolds numbers (Re) and Mach numbers (M) up to 1.15×10^6 and 0.26 respectively (U_∞ = 93 m/s). The control mechanism of the NS-DBD actuators does not appear to be momentum addition, unlike the case with AC-DBD plasmas. Instead, rapid localized heating of the fluid near the surface of the actuator is believed to provide the excitation. This localized heating creates compression waves that propagate into the flow and act as a perturbation. Two control mechanisms are found, depending upon the Re and α. At low Re (0.25×10^6) and angles of attack just past stall, the NS-DBD actuator acts as an active boundary layer trip. At higher flow speeds ($Re = 1.15 \times 10^6$, $M = 0.26$) and angles of attack, the NS-DBD plasma actuator excites natural flow instabilities that develop into large coherent structures. These structures increase the momentum in the near wall fluid by entraining high momentum fluid from the freestream. The efficacy of this control mechanism is dependent on the frequency of actuation with the best results obtained at $F^+ \approx 2$.

NS-DBD plasma actuators are used in conjunction with constant voltage hot film anemometers in closed-loop separation control. Two types of closed-loop control are demonstrated. On/off control uses the mean value of power dissipated by a hot film on the pressure side of the airfoil near the leading edge (x/c = 11%). This serves as an input to the controller by sensing changes in the stagnation line location which correlate with C_L. The on/off controller is most useful at low Re and moderate α. In this case, the control mechanism is an active boundary layer trip. This logic allows the controller to turn off the plasma for periods of time where hysteresis effects keep the flow attached to the airfoil, thereby reducing power consumption. The on/off controller is also used in flow conditions where the excitation of flow instabilities is necessary (high Re, high α). In this regime the actuator must remain on constantly to avoid high unsteady loading on the airfoil. Extremum-seeking control is used to optimize the forcing frequency of the actuator during dynamic variation of Re. In this preliminary work, the controller performance is not consistent, presumably due to sub-optimal hot film sensor location. The mixed success of the closed-loop controllers notwithstanding, several challenges typically associated with integration of DBD plasma actuators into a feedback control system have been overcome. The most important of these is the demonstration of control authority at realistic takeoff and approach Re and M. Many remaining challenges are currently being addressed.

Acknowledgments

This work was funded in part by the Air Force Research Laboratory Air Vehicles Directorate with Dr. Jonathan Poggie. Additional funding was provided by the Ohio State University. Two undergraduate students, Chris Wiet and Troy Niekamp, were very helpful in this work and their help is appreciated.

References

[1]Greenblatt, D. and Wygnanski, I., "The Control of Flow Separation by Periodic Excitation," *Progress in Aerospace Sciences*, Vol. 36, 2000, pp. 487-545.

[2]McLean, J., Crouch, J., Stoner, R., Sakurai, S., Seidel, G., Feifel, W. and Rush, H., "Study of the Application of Separation Control by Unsteady Excitation to Civil Transport Aircraft," NASA CR-209338, 1999.

[3]Patel, M., Sowle, Z., Corke, T. and He, C., "Autonomous Sensing and Control of Wing Stall Using a Smart Plasma Slat," *Journal of Aircraft*, Vol. 44, No. 2, 2007, pp. 516-527.

[4]Samimy, M., Debiasi, M., Caraballo, E., Serrani, A., Yuan, X., Little, J. and Myatt, J., "Feedback control of subsonic cavity flows using reduced-order models," *Journal of Fluid Mechanics*, Vol. 579, 2007, pp. 315-346.

[5]Pinier, J., Ausseur, J., Glauser, M. and Higuchi, H., "Proportional Closed-Loop Feedback Control of Flow Separation," *AIAA Journal*, Vol. 45, No. 1, 2007, pp. 181-190.

[6]Becker, R., King, R., Petz, R. and Nitsche, W., "Adaptive Closed-Loop Separation Control on a High-Lift Configuration using Extremum Seeking," *AIAA Journal*, Vol. 45, No. 6, 2007, pp. 1382-1392.

[7]Poggie, J., Tillman, C., Flick, P., Silkey, J., Osborne, B., Ervin, G., Maric, D., Mangalam, S. and Mangalam, A., "Closed-Loop Stall Control System," *Journal of Aircraft*, Vol. 47, No. 5, 2010, pp. 1747-1755.
[8]Sinha, A., Kim, K., Kim, J., Serrani, A. and Samimy, M., "Extremizing Feedback Control of a High-Speed and High Reynolds Number Jet," *AIAA Journal*, Vol. 48, No. 2, 2010, pp. 387-399.
[9]Benard, N., Moreau, E., Griffin, J. and Cattafesta, L., "Slope Seeking for Autonomous Lift Improvement by Plasma Surface Discharge," *Experiments in Fluids*, Vol. 48, 2010, pp. 791-808.
[10]Glezer, A. and Amitay, M. "Synthetic Jets,"*Annual Review of Fluid Mechanics*, Vol. 34, No. 2002, pp. 503-529.
[11]Corke, T., Post, M. and Orlov, D., "Single Dielectric Barrier Discharge Plasma Enhanced Aerodynamics: Physics, Modeling and Applications," *Experiments in Fluids*, Vol. 46, 2009, pp. 1-26.
[12]Moreau, E., "Airflow Control by Non-Thermal Plasma Actuators," *Journal of Physics D: Applied Physics*, Vol. 40, 2007, pp. 605-636.
[13]Forte, M., Jolibois, J., Pons, J., Moreau, E., Touchard, G. and Cazalens, M., "Optimization of a Dielectric Barrier Discharge Actuator by Stationary and Non-Stationary Measurements of the Induced Flow Velocity: Application to Airflow Control," *Experiments in Fluids*, Vol. 43, 2007, pp. 917-928.
[14]Macheret, S., Shneider, M., Miles,R., "Magnetohydrodynamic and Electrohydrodynamic Control of Hypersonic Flows of Weakly Ionized Plasmas," *AIAA Journal,* Vol. 42, No. 7, 2004, pp. 1378-1387.
[15]Thomas, F., Corke, T., Igbal, M., Kozlov, A. and Schatzman, D., "Optimization of Dielectric Barrier Discharge Plasma Actuators for Active Aerodynamic Flow Control," *AIAA Journal*, Vol. 47, No. 9, 2009, pp. 2169-2178.
[16]Roupassov, D., Nikipelov, A., Nudnova, M. and Starikovskii, A., "Flow Separation Control by Plasma Actuator with Nanosecond Pulsed-Periodic Discharge," *AIAA Journal*, Vol. 47, No. 1, 2009, pp. 168-185.
[17]Samimy, M., Kim, J.-H., Kastner, J., Adamovich, I. and Utkin, Y., "Active Control of High-Speed and High-Reynolds-Number Jets using Plasma Actuators," *Journal of Fluid Mechanics*, Vol. 578, 2007, pp. 305-330.
[18]Gaitonde, D., "Simulation of Supersonic Nozzle Flows with Plasma-based Control," *AIAA 39th Fluid Dynamics Conference*, AIAA Paper 2009-4187, 2009.
[19]Little, J., Takashima, K., Nishihara, M., Adamovich, I. and Samimy, M., "High Lift Airfoil Leading Edge Separation Control with Nanosecond Pulse Driven DBD Plasma Actuators," *AIAA 5th Flow Control Conference*, AIAA Paper 2010-4256, 2010.
[20]Takashima, K., Y. Zuzeek, Lempert, W., Adamovich, I., "Characterization of Surface Dielectric Barrier Discharge Plasma Sustained by Repetitive Nanosecond Pulses," *AIAA 41st Plasmadynamics and Lasers Conference*, AIAA Paper 2010-4764 2010.
[21]Seifert, A., Darabi, A. and Wygnanski, I., "Delay of Airfoil Stall by Periodic Excitation," *Journal of Aircraft*, Vol. 33, No. 4, 1996, pp. 691-698.
[22]N. Benard, J. P. Bonnet, E. Moreau, J. Griffin, and L. N. Cattafesta, III, "On the Benefits of Hysteresis Effects for Closed-Loop Separation Control Using Plasma Actuation," *AIAA 5th Flow Control Conference*, AIAA Paper 2010-4259, 2010.